The Journal of Chemical Physics

Plasmon-induced efficient hot carrier generation in graphene on gold ultrathin film with periodic array of holes: Ultrafast pump-probe spectroscopy

Cite as: J. Chem. Phys. **151**, 234712 (2019); https://doi.org/10.1063/1.5117882
Submitted: 04 July 2019 • Accepted: 25 November 2019 • Published Online: 17 December 2019

Gyan Prakash, Rajesh Kumar Srivastava, Satyendra Nath Gupta, et al.

COLLECTIONS

Paper published as part of the special topic on Emerging Directions in Plasmonics

View Online Export Citation CrossMark

ARTICLES YOU MAY BE INTERESTED IN

Special topic on emerging directions in plasmonics
The Journal of Chemical Physics **153**, 010401 (2020); https://doi.org/10.1063/5.0017914

Plasmonic hot electrons for sensing, photodetection, and solar energy applications: A perspective
The Journal of Chemical Physics **152**, 220901 (2020); https://doi.org/10.1063/5.0005334

Dark plasmon modes for efficient hot electron generation in multilayers of gold nanoparticles
The Journal of Chemical Physics **152**, 064710 (2020); https://doi.org/10.1063/1.5131696

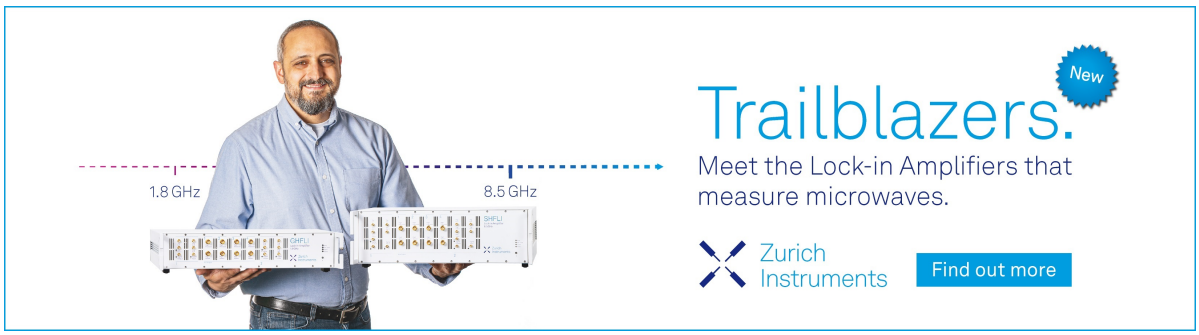

AIP Publishing

© 2019 Author(s).

The Journal of Chemical Physics ARTICLE scitation.org/journal/jcp

Plasmon-induced efficient hot carrier generation in graphene on gold ultrathin film with periodic array of holes: Ultrafast pump-probe spectroscopy

Cite as: J. Chem. Phys. 151, 234712 (2019); doi: 10.1063/1.5117882
Submitted: 4 July 2019 • Accepted: 25 November 2019 •
Published Online: 17 December 2019

View Online Export Citation CrossMark

Gyan Prakash,[1,2] Rajesh Kumar Srivastava,[1] Satyendra Nath Gupta,[1] and A. K. Sood[1,2,a)]

AFFILIATIONS

[1] Department of Physics, Indian Institute of Science, Bangalore 560 012, India
[2] Center for Ultrafast Laser Application, Indian Institute of Science, Bangalore 560 012, India

Note: This paper is part of the JCP Special Topic on Emerging Directions in Plasmonics.
[a)] **Electronic mail:** asood@iisc.ac.in

ABSTRACT

Using ultrafast pump-probe reflectivity with a 3.1 eV pump and coherent white light probe (1.1–2.6 eV), we show that graphene on gold nanostructures exhibits a strong coupling to the plasmonic resonances of the ordered lattice hole array, thus injecting a high density of hot carriers in graphene through plasmons. The system being studied is single-layer graphene on an ultrathin film of gold with periodic arrangements of holes showing anomalous transmission. A comparison is made with gold film with and without hole array. By selectively probing transient carrier dynamics in the spectral regions corresponding to plasmonic resonances, we show efficient plasmon induced hot carrier generation in graphene. We also show that due to high electromagnetic field intensities at the edge of the submicron holes, fast decay time (10–100 fs), and short decay length (1 nm) of plasmons, a highly confined density of hot carriers (very close to the edge of the holes) is generated by Landau damping of plasmons within the holey gold film. A contribution to transient decay dynamics due to the diffusion of the initial nonuniform distribution of hot carriers away from the hole edges is observed. Our results are important for future applications of novel hot carrier device concepts where hot carriers with tunable energy can be generated in different graphene regions connected seamlessly.

Published under license by AIP Publishing. https://doi.org/10.1063/1.5117882

I. INTRODUCTION

Surface plasmon polaritons (SPPs) due to their inherent property of nanoscale confinement and localization, smaller than the interacting light wavelength, show strong light-matter interaction. This leads plasmonics to a wide variety of applications from efficient harvesting of solar energy to nanoscale optical devices.[1–3] Efficient generation and transfer of hot electron-hole pairs have been at the heart of efficient conversion of solar energy in photovoltaic and photocatalytic devices.[4] Plasmons in nanostructures decay through Landau damping (with damping time of few tens of femtoseconds[5–8]) to generate energetic electrons, with energies larger than those of the thermal excitation (known as the hot electrons) at ambient temperatures.[9–14] Hot carriers can be accessed through plasmon induced hot-electron charge transfer into adjacent interface materials.[7,10,15,16] If a high conductance pathway is available, the plasmon generated hot electrons can rapidly conduct over long distances, which might also discourage the electrons once transferred from returning to the plasmonic material. In graphene, electrons move with high velocities ($v_F = 10^6$ m/s) and behave like massless fermions, making it the most desirable material for the high-speed electronics and optoelectronics applications. A substantial challenge to the performance of most of

Published under license by AIP Publishing

the graphene-based optoelectronic devices[17–19] comes from the weak absorption of light (only 2.3% at normal incidence) in graphene. Thus, efficient hot electron injection in graphene through plasmons gains valuable importance. Graphene in a hybrid plasmonic structure is a promising element for high-speed electrically controllable optical and optoelectronic devices. Two dominant mechanisms to induce hot carriers in graphene are (i) direct hot electron transfer by Landau damping of plasmons in Au nanostructures, as seen in reduced graphene oxide coated gold nanoparticles[20] and graphene covered gold nanorods,[21] and (ii) generation of carriers by the near field enhanced electric field, as reported in graphene covered nanodisks.[22] Ultrafast pump-probe experiments have played an important role in identifying the hot carrier transfer mechanism and dynamics.[10,23,24]

Ever since the phenomenon of extraordinary optical transmission (EOT) was demonstrated,[1,25] plasmonic structures with a periodic array of holes in metal films owing to high refractive index sensitivity (RIS) and tunable plasmonic properties have found wide applications from optical elements to chemical and biological sensors.[26–28] Graphene on plasmonic nanostructures of noble metals is the simplest and effective hybrid structure for seamless integration of graphene with plasmons. Recent experiments have shown a strong light-graphene interaction enhanced by plasmons of an array of holes and nanovoids in gold.[29,30] Of particular interest are the nanovoids with protruding edges which show strong graphene-plasmon interaction due to a relatively large interaction area between graphene and the strong electric field of plasmons at the voids or rims. Despite having the possibility of more strong interaction of graphene on 3D hole arrays due to large interaction area (similar to the case of nanovoids) and enhanced field intensities (because of matched plasmon energy between the two sides), this has not been explored. Most of the studies of graphene-covered periodic hole/nanovoid arrays so far have focused on the enhanced environmental sensitivity of plasmonic resonances.[29–35] The ultrafast interplay of the dynamics of carriers and plasmons in the graphene-covered metal hole array is completely unexplored.

Here, we show that a high density of hot-electrons can be generated in graphene through a strong interaction in a hybrid plasmonic structure of graphene with a 3D gold hole array. Using ultrafast pump pulses (~80 fs) of energy 3.1 eV, we photoexcite carriers in the graphene-gold hole array hybrid system and probe their relaxation dynamics with coherent white light in the spectral window of 1.1 eV–2.6 eV. Notably, pump-induced reflectivity shows significant signatures in the spectral window corresponding to EOT resonances of the gold hole array originating from the carrier dynamics in graphene. A comparative study of the graphene on the gold film with and without hole array confirms the highly efficient direct plasmon induced hot carrier generation in graphene.

II. EXPERIMENTAL AND SIMULATION DETAILS

The gold hole array was fabricated on a glass substrate by a colloidal lithography technique.[36] The hole array was prepared by spin coating the solution of polystyrene spheres of 1 μm mean diameter on a glass substrate for a hexagonal close-packed colloidal monolayer. The polystyrene sphere diameter was reduced to about 480 nm with reactive ion etching using the O_2 plasma. Subsequently, the 50 nm Au with 5 nm Ti adhesion layer was deposited on the microspheres by sputtering. The removal of polystyrene spheres by ultrasonication gives holes of 490 ± 30 nm diameter in the gold film. The atomic force microscopy (AFM) and scanning electron microscopy (SEM) were used to characterize the morphology of the fabricated hole array [see Figs. 1(a) and 1(b)]. The array of holes with an

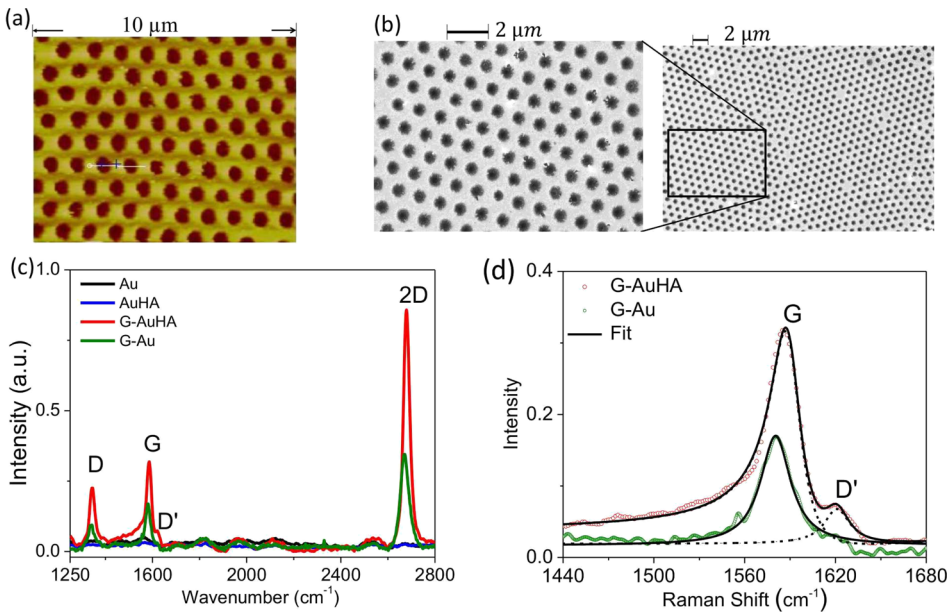

FIG. 1. (a) AFM and (b) SEM images of the ordered triangular lattice array of holes. (c) Raman spectrum of single layer graphene transferred on AuHA and Au. (d) Asymmetric line shape of the G band in G-AuHA compared with the G band of G-Au. The solid line in G-Au is fit to the experimental data with a Lorentzian, whereas that in G-AuHA is with the Breit-Wigner-Fano (BWF) line shape.

Published under license by AIP Publishing

average diameter of 490 nm are arranged in a triangular lattice of 1 μm periodicity.

Single-layer graphene samples were grown on a 25 μm thick copper foil by the chemical vapor deposition technique and transferred on gold films with and without hole array by the conventional technique.[37,38] The PMMA on the graphene was removed by immersing the substrate in acetone at 60 °C, followed by annealing for 3 h at 500 °C under hydrogen and argon atmospheres. For a reference, the Au film of 50 nm thickness without hole array with Ti adhesion layer was deposited on a glass substrate. We have studied four samples: (i) 50 nm gold film with hole array (AuHA), (ii) graphene covered gold hole array (G-AuHA), (iii) 50 nm gold film (Au), and (iv) graphene covered 50 nm gold film (G-Au).

Figure 1(c) shows the Raman spectrum of G-AuHA and G-Au with an excitation wavelength of 532 nm. The peak positions of G mode (1590 cm^{-1}) and 2D mode (2680 cm^{-1} with a width of ~31 cm^{-1}) and their intensity ratio confirm the single layer graphene on G-AuHA.[39] The D band intensity with respect to the G-band (I_D/I_G ~ 0.68) shows the presence of disorder in the single layer graphene. The D′ band (1621 cm^{-1}) associated with the disorder activated longitudinal optical phonons near Γ-point is also seen in G-AuHA. As the work function of graphene (~4.56 eV[40]) is lower than that of gold (~4.83 eV[41]), graphene on the gold film gets p-doped. Furthermore, CVD grown graphene gets unintentionally p-doped due to charge transfer from atmospheric H_2O/O_2 molecules. The intensity ratio I(2D)/I(G) is ~2.7 and 2.0 for graphene on AuHA and graphene on Au, respectively. From the I(2D)/I(G) ratio, we find that graphene on Au is more p-doped than graphene on AuHA with Fermi energies at −352 meV and −206 meV, respectively.[39] This is commensurate with the fact that graphene is relatively in more contact with gold in the case of G-Au than G-AuHA. A enhancement of ~2 in Raman intensity of D, G, and 2D modes in G-AuHA in comparison to G-Au is due to the enhanced electric field originating from the nanostructure.[29] The G band of G-AuHA shows an asymmetric line shape [Fig. 1(d)]. We fit the G band with the Breit-Wigner-Fano (BWF) line shape:[42] $I(\omega) = I_0[1 + (\omega - \omega_G)/q\Gamma]^2/[1 + [(\omega - \omega_G)/\Gamma]^2]$ (where Γ is the linewidth, ω_G is the G band frequency, and 1/q is the interaction parameter between the phonon and electronic continuum). From the fit, we obtain ω_G = 1590.0 ± 0.3 cm^{-1}, Γ = 12.1 ± 0.3 cm^{-1}, and −1/q = 0.23 ± 0.01. From the Lorentzian fit to the symmetric G band in G-Au, the values are ω_G = 1580.0 ± 0.1 cm^{-1} and Γ = 12.0 ± 0.2 cm^{-1}. Similar values of 1/q as seen by us have been reported for metallic single-walled carbon nanotubes (SWNTs) where a lower frequency (G band) transverse optical (TO) phonon component couples to the 1D-π plasmons.[43] Asymmetric line shapes have been observed in graphene as a manifestation of a Fano resonance originating from the interaction of G-phonons with the excitonic states formed in undoped graphene.[44] The interaction parameter 1/q observed by us is about a factor of 3 greater than that observed in pristine graphene with Fermi energy at the charge neutrality point.[44] We attribute the observed BWF line shape to the interaction of G phonons with the electronic Raman background of AuHA, implying strong coupling of graphene with the plasmonic nanostructure.

Transient reflectivity measurements were done by exciting the samples with 80 fs pulses of central wavelength 400 nm (3.1 eV), obtained by frequency doubling 800 nm (1.57 eV) derived from Ti:sapphire amplifier (Spitfire from Spectra Physics, Inc.) with a BBO crystal. Pump-induced reflectivity changes were monitored for Au, G-Au, AuHA, and G-AuHA with a stable white light probe (generated by focusing a small fraction of 800 nm on a sapphire crystal) in a spectral window of 1.1 eV–2.6 eV. Pump beam with a fluence of 138 $\mu J/cm^2$ (for Au, AuHA, and G-AuHA) and 201 $\mu J/cm^2$ (for G-Au) with an incident angle of ~14° was used.

The steady state transmission measurements were done using a UV/VIS spectrophotometer (Lambda 950 Perkin Elmer). Optical transmission of the AuHA and G-AuHA is simulated using the 3D full wavevector FDTD method using the software package (FDTD Solutions from M/s Lumerical, Inc.). A plane polarized source with polarization along the x-axis propagating in the z-direction normal to AuHA and G-AuHA is considered. A transmission intensity monitor at the back side and a field intensity monitor at the front surface of AuHA and G-AuHA were kept to record the simulated light transmission and the electric field intensity at the surface, respectively. For accounting the irregularities in the circular shape of holes and better agreement with the experimentally observed transmission, the simulated transmission was averaged over transmission spectra from slightly elliptical holes (keeping the sum of major and minor axis radii 500 nm) with the same periodicity.

III. RESULTS AND DISCUSSION

Figure 2(a) shows the measured transmission spectra of AuHA and G-AuHA showing extraordinary optical transmission (EOT) peaks due to the triangular lattice array of holes. For comparison, the transmission spectrum of the gold film of the same thickness is also shown. The transmission spectrum of AuHA and G-AuHA is not vertically shifted in Fig. 2(a), thus showing enhanced transmission with respect to Au. Transmission spectra of AuHA and G-AuHA show three EOT transmission peaks whose positions are related to the lattice constant a_0 of the hole array, dielectric constants of the surrounding medium (ε_d) and the metal (ε_m), and the Bragg resonance order (i, j) of the SPPs satisfying Bragg condition,[1]

$$\nu_{max}^{(i,j)} = ca_0^{-1}\left[(4/3)\left(i^2 + ij + j^2\right)\left(\varepsilon_m^{-1} + \varepsilon_d^{-1}\right)\right]^{1/2}. \quad (1)$$

We observe three EOT peaks in the transmission spectrum at 0.6 eV, 1.0 eV, and 1.4 eV, marked as G1, G2, and G3 in Fig. 2(a), respectively. The observed EOT peak positions are in good agreement with the reports on similar gold hole array films.[45,46] The simulated transmission spectrum for the triangular lattice gold hole array of 500 nm diameter and 1000 nm periodicity on the glass substrate is shown in Fig. 2(b). This guides us in assigning the EOT peaks as follows (Table I): the transmission peak G1 is due to the (1,0) AuHA/glass Bragg resonance order, the broad EOT peak G2 is due to the overlap of (1,0)* Air/AuHA and (1,1) AuHA/glass resonance peaks, and the G3 peak is attributed to the (2,0) AuHA/glass resonance peak. A slight blue shift of the simulated spectrum with respect to the measured one can be due to the irregularities in the long range periodicity of the triangular lattice of the hole arrays, which has not been considered in the simulation. An overall enhanced transmission of ~10% in AuHA with respect to Au is observed in the spectral window from 1.6 eV to 4.0 eV where EOT peaks are not seen. G-AuHA due to absorption

Published under license by AIP Publishing

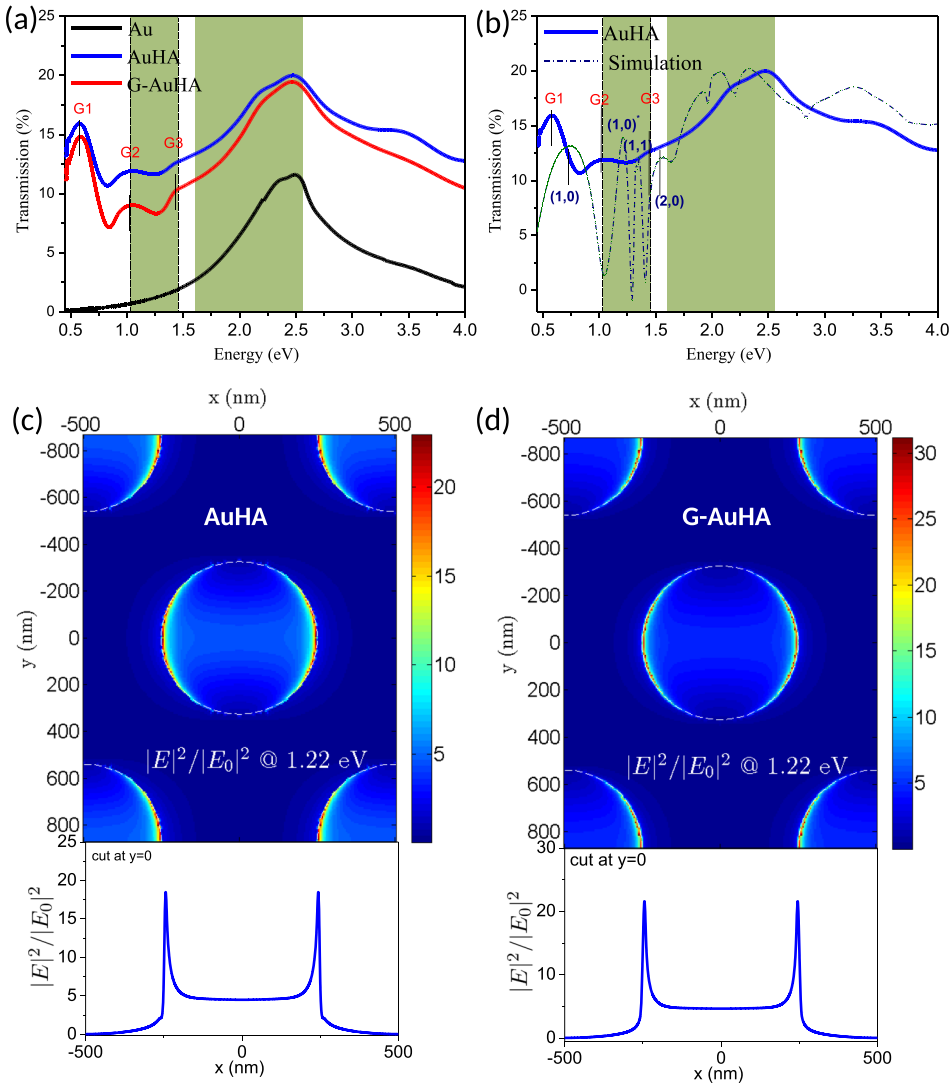

FIG. 2. (a) Transmission spectrum of AuHA and G-AuHA showing extraordinary optical transmission (EOT) peaks due to the coupling of light with the plasmonic resonances of the ordered lattice hole array. Respective plasmonic mode indices are also indicated. For comparison, the transmission spectrum of the gold film (Au) of the same thickness is also included (the plots are not shifted vertically). (b) FDTD simulated transmission spectrum showing (1,0) AuHA/glass, (1,0)* Air/AuHA, (1,1) AuHA/glass, and (2,0) AuHA/glass interface EOT peaks. For comparison, experimental AuHA transmission data in (a) are also included. Green shaded regions refer to the spectral window covered by the white light probe in the transient differential reflectivity measurement experiment. (c) and (d) Electric field intensity profile and plot at y = 0 for EOT (1,0)* Air/AuHA and (1,0)* Air/G-AuHA at 1.22 eV, respectively.

in graphene (2.3%) shows a slightly reduced transmission with respect to AuHA in the same spectral window. However, in the spectral window of 0.5 eV–1.6 eV at EOT peaks, due to the coupling of graphene with the plasmonic modes, transmission is reduced by ~3.5%.[29,30]

The simulations with graphene on top of the AuHA did not show any difference in the transmission peak positions. However, the electric field intensity is enhanced due to graphene by more than ~55%. Figures 2(c) and 2(d) show the simulated electric field intensity distribution profile on the top surface of AuHA and

TABLE I. Electric field intensity ratio *R* for EOT frequencies observed in the FDTD simulated transmission spectrum of AuHA and G-AuHA.

Calculated EOT peak position (eV)		Assignment	*R* (AuHA)	*R* (G-AuHA)	Enhancement (%)
0.83	G1	(1,0) AuHA/glass	369	543	47
1.22	G2	(1,0)* Air/AuHA	562	869	55
1.35	G2	(1,1) AuHA/glass	159	276	74
1.55	G3	(2,0) AuHA/glass	7.8	8.7	11

Published under license by AIP Publishing

G-AuHA, respectively, for the photon energy corresponding to (1,0)* Air/AuHA and (1,0)* Air/G-AuHA EOT resonance frequencies. The electric field intensity profiles show that the field intensity is high at the edge of the holes [see electric field intensity plots at y = 0 in Figs. 2(c) and 2(d)]. Table I summarizes the calculated intensity ratio $R = |E|^2_{edge}/|E|^2_{mid}$, where $|E|^2_{edge}$ and $|E|^2_{mid}$ are the electric field intensities at the edge and at a midpoint between the two adjacent holes. It can be seen that the electric field intensities at the hole edge are higher at G1 and G2 EOT frequencies. The (1,0)* Air/AuHA shows a greater $|E|^2_{edge}/|E|^2_{mid}$ value than the (1,0) AuHA/glass as the SPP is on the Air/AuHA interface, where the near field monitor is placed. The corresponding electric field intensities are enhanced when AuHA is covered with graphene (see Table I). We will see later that the intense electric field intensities at the edge of the holes play an important role in hot carrier generation in graphene.

Figure 3(a) shows a transient pump-induced reflectivity change as a function of probe energy in Au, AuHA, G-Au, and G-AuHA at a probe delay of 1 ps in the spectral window of 1.1–1.45 eV (NIR) and 1.7–2.8 eV (UV-VIS). The observed pump induced reflectivity change matches qualitatively in all four samples. The shape of the reflectivity change as a function of probe energy depends on the different regions of electronic density of states (DOS) interrogated by the probe pulse [as illustrated in Fig. 4(d)].[47] The pump beam at 3.1 eV (higher than the interband transition of gold at 2.4 eV) gets absorbed by the 5d → 6s transition and excites the electron distribution out of equilibrium in the conduction band and holes in the 5d band. From the two-photon photoemission (2PPE) studies, it has been seen that the holes in the 5d state relax in a very short time, of the order of few tens of femtoseconds, via Auger processes and deliver the excess energy to the 6s band electrons.[47–50] Thus, the excited 5d holes relax within the pump pulse duration. The non-Fermi electron distribution, through electron-electron interaction, redistributes its energy and attains a Fermi distribution with temperature $T_e \gg T_0$ (initial lattice temperature). The thermalization time of electrons varies from <100 fs to few hundreds of femtoseconds.[51,52] The quasithermalized electron distribution then loses its energy within a few picoseconds to the lattice through electron-phonon interaction. An equilibrium with the lattice at a slightly higher temperature than T_0 is reached afterward followed by cooling of the hot lattice on a 100 ps time scale.[51,53] Following the arguments of Sun *et al.*, the nonthermalized distribution of carriers interacts with the phonon bath during the thermalization process. Therefore, exploring the energy exchange mechanism by considering the onset of the electron-electron and electron-phonon relaxation as two separate regimes is not accurate. However, the energy exchange mechanism can be modeled by taking two separate populations of photoexcited carriers of thermalized and nonthermalized distributions.[51] Following Ref. 51, we fit the transient reflectivity with the following function convoluted with the Gaussian pulse

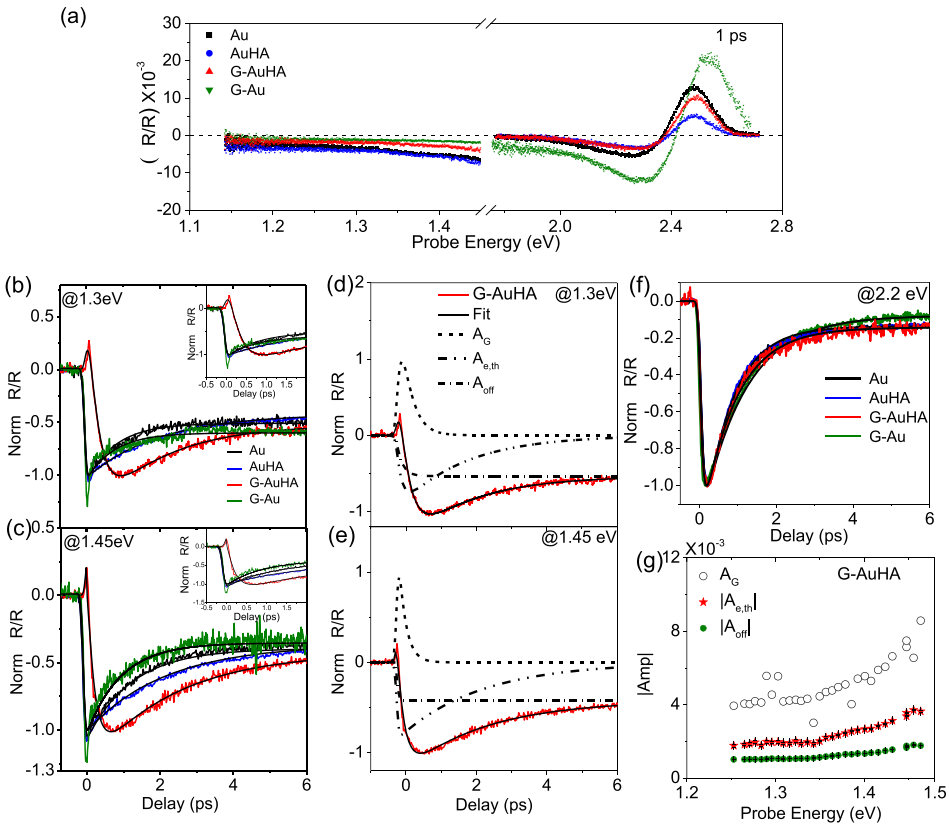

FIG. 3. (a) 400 nm (3.1 eV) pump induced reflection change of Au, AuHA, G-AuHA, and G-Au at 1 ps probe delay. Kinetics of Au, AuHA, G-AuHA, and G-Au at probe energies (b) 1.3 eV and (c) 1.45 eV. Solid lines are fit to the experimental data, as discussed in the main text. Inset in (b) and (c) shows the zoomed kinetics up to 2 ps delay at probe energies 1.3 eV and 1.45 eV, respectively. [(d) and (e)] Fitting components contributing to the total fit of the kinetics of G-AuHA in (b) and (c). (f) Kinetics at probe energy 2.2 eV compared for all four samples. The plasmon induced signal originating from graphene is not observed in the probe region where plasmonic resonances are not present. (g) Amplitude of the fitting components as a function of probe energy in G-AuHA.

Published under license by AIP Publishing

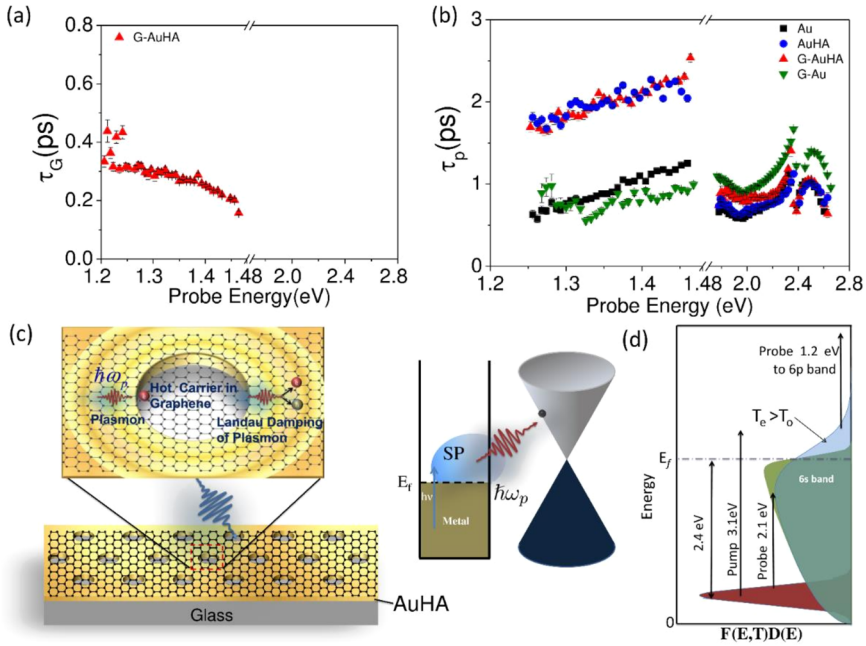

FIG. 4. (a) Decay time constant τ_G of plasmon induced hot carriers generated in graphene through carrier-optical phonon scattering as a function of probe energy. (b) Probe photon energy dependence of phonon mediated carrier relaxation time in Au, AuHA, G-AuHA, and G-Au. (c) Schematic showing plasmon induced hot electron generation in graphene by charge transfer from Au to graphene and Landau damping of plasmons creating electron-hole pairs (d) Illustration qualitatively showing electronic density of states of gold (adopted from Ref. 47). Excited electrons after thermalization attain an electronic temperature much higher than the lattice temperature. Fermi-Dirac distribution of electrons at an elevated temperature smears carrier occupancies around Fermi energy (E_f). Probe with energy less than interband transition threshold ~2.4 eV detects holes below fermi energy.

response,

$$\frac{\Delta R}{R}(\hbar\omega, t) = \mathrm{H}(t)\left\{A_{e,NT}e^{-t/\tau_{r'}} + A_{e,th}\left(1 - e^{-t/\tau_r}\right)e^{-t/\tau_p} + A_G e^{-t/\tau_G} + A_L\right\}, \quad (2)$$

where H(t) is a Heaviside step function. $A_{e,NT}$ and $A_{e,th}$ are the initial transient amplitudes corresponding to nonthermalized and thermalized electronic distributions in Au, respectively. A_L is the offset amplitude due to slow cooling of the lattice. τ_r and τ_p are the rise time associated with the thermalization of photoexcited carriers and the time constant for the decay of the thermalized distribution due to electron-phonon interaction, respectively. $\tau_{r'} = (1/\tau_r + 1/\tau_p)^{-1}$ is the decay time of nonthermalized population, taking into account simultaneous interaction of nonthermalized electrons with the phonon bath. A_G and τ_G are the amplitude and decay time of the signal from graphene considered only in the NIR region, respectively. As the amplitude of nonthermalized distribution is shown to be significant only around Fermi energy (~2.4 eV) of gold,[51] we include the contribution of $A_{e,NT}$ only near 2.4 eV probe energy. Except for the probe energy ~2.4 eV, the rise time τ_r in all four samples is limited by the instrument response function (~115 fs). The rise time τ_r is found to be ~250 fs near Fermi energy of gold. The long rise time observed near Fermi energy is due to the state filling effect,[51] which blocks the relaxation of electrons close to the Fermi surface, while high-energy electrons decay on a much shorter time scales. This is also commensurate with the Fermi liquid theory which predicts that the relaxation rate varies as $(E - E_f)^2$.[51]

Figures 3(b) and 3(c) show a comparison of the kinetics of photoexcited carriers in G-AuHA with AuHA, G-Au, and Au at two representative central probe energies 1.3 and 1.45 eV in the NIR region. For better S/N ratio and improved fitting, the kinetic traces have been averaged with a window of $\Delta E \sim 6$ meV. The behavior of G-AuHA kinetics in this region compels us to consider an additional exponentially decaying component ($A_G e^{-t/\tau_G}$) with positive amplitude A_G and decay time τ_G in the fitting function [Eq. (2)]. The positive signal contributing to $\Delta R/R$ is related to the transient carrier dynamics of plasmon induced hot carriers in graphene. The positive sign of the signal originating from graphene is in agreement with the reported ultrafast study of graphene.[22] No such positive signal in the UV-VIS region is observed for G-AuHA [Fig. 3(f)]. It can be seen from the fits that the dynamics is well described by the function [see Figs. 3(d) and 3(e)]. The fit to the experimental data was found to be excellent over the entire probe energies. Figure 3(g) shows the amplitudes A_G as a function of probe photon energy together with $A_{e,th}$ and A_G in G-AuHA. The relaxation time constants obtained from the fit are shown in Figs. 4(a) and 4(b).

We see that as the probe photon energy increases from 1.2 to 1.45 eV, τ_G decreases from 350 ± 50 fs to 200 ± 20 fs. The decay time agrees well with the characteristic decay time of carriers through electron-optical phonon (e-op) scattering in CVD grown graphene.[54,55] The e-op scattering in graphene is mainly due to zone-boundary optical phonons, and the decay rate is given by $\frac{1}{\tau_G} = \frac{2\pi}{\hbar}|\varepsilon|W$.[54,56] Here, $|\varepsilon| = E - E_f$ is the electron energy with respect to Fermi energy. W is the dimensionless electron-phonon coupling constant. The characteristic decay time, its dependence on probe photon energy, and e-op coupling constant obtained experimentally confirm that the positive signal seen in the hybrid G-AuHA structure in the NIR region originates from the carrier dynamics in graphene. As the additional signal is observed only in the G-AuHA sample in the NIR region having the plasmonic resonances due to the hole array [resonances G1, G2, and G3 in Fig. 2(a)], we attribute the amplitude A_G due to transient reflectivity modulated by plasmon induced hot carriers in the graphene with τ_G as their

Published under license by AIP Publishing

relaxation time.[20–22] Schematic in Fig. 4(c) illustrates the hot carrier generation mechanism in graphene. As the pump beam is not in resonance with the EOT peaks (G1, G2, and G3), the induced hot carriers in graphene cannot be due to the near field enhanced direct photoexcitation.[22] The generation of hot carriers in graphene is due to plasmon induced interfacial hot carrier transfer from Au into the graphene through regions in contact with the protruding edges of the nanoholes having high near field intensities.[10]

In the discussion that follows, we examine the relaxation time of thermalized carriers in gold through electron-phonon scattering τ_p and its dependence on probe energy as shown in Fig. 4(b). We see that τ_p in the UV-VIS region shows a similar behavior for Au and AuHA. Interestingly, there is a two fold increase in τ_p in the NIR region. The presence of graphene in G-Au and G-AuHA has no effect on τ_p in gold, as expected. The spectral dependence of the different regions probed in the electronic band structure of gold is schematically shown in Fig. 4(d).[47] We will first discuss the dependence of τ_p in the UV-VIS range. τ_p increases from 0.8 ps at 2.0 eV to 1.2 ps at 2.4 eV and then decreases as probe energy further increases beyond 2.4 eV–2.8 eV. As the crystal structure of gold has only one atom per unit cell, carrier relaxes through acoustic phonon emission. The decay time varies as $\sim \sqrt{k_B T_L/E}$, where E is the energy of electrons, k_B is the Boltzmann constant, and T_L is the lattice temperature.[57] The smearing of Fermi-Dirac distribution of the electrons at the elevated electron temperature T_e creates holes below the Fermi energy. As a consequence of this, the forbidden interband transition 5d → 6s states below the Fermi energy at initial electron temperature $T_e = T_0$ are allowed at $T_e \gg T_0$, whereas the states above the Fermi energy are blocked by the phase space filling.[47] Therefore, the probe photons with energy less than the interband transition threshold ($E_{pr} \sim 2.4$ eV) detect holes below Fermi energy, whereas those greater than the interband transition threshold detect electrons above Fermi energy. Hence, the observed electron-phonon cooling rate is higher when probed at 2.0 eV, increases with probe photon energy up to $E_f \sim 2.4$ eV, and then decreases as probe photon energy moves away from the Fermi energy up to 2.8 eV.

In the NIR region, there are three main results: (i) an overall increase of 1 ps in τ_p of AuHA as compared to Au, (ii) the linear increase in τ_p with probe photon energy, and (iii) as mentioned before, the presence of graphene in G-Au and G-AuHA has no effect on τ_p. As the probe in the NIR region corresponds to intraband transition, one would expect photobleach signal ($\Delta R/R$ with a positive sign) due to the thermalized distribution of carriers near E_f. However, as the observed $\Delta R/R$ signal in this region is negative, a photoinduced absorption is possible due to the transition from 6s band to 6p band.[58,59] The probe in this region is excited state absorption by the thermalized carriers above E_f and detects the electron with energy $E = E_{6p} - E_{pr}$, where $E_{6p} \sim 4.32$ eV[58] is the position of the 6p band and E_{pr} is the probe photon energy. Higher energy probe photons therefore detect low energy electrons above the Fermi energy. As discussed earlier, the thermalized electrons decay through acoustic phonons with decay time-varying as $\sim \sqrt{k_B T_L/E}$, τ_p is expected to vary as $\sim \sqrt{k_B T_L/(E_{6p} - E_{pr})}$. Therefore, in this region, we see τ_p increasing with probe photon energy.

We now look at an overall increase in τ_p by 1 ps in AuHA in the NIR region. The perforation of the gold film with holes cannot change the electron-phonon coupling constant of gold, and hence, the increase in τ_p cannot be associated with change in shape or filling factor.[60] However, the plasmonic behavior of AuHA can alter the relaxation time τ_p. In the NIR region, as the plasmons decay through the Landau damping mechanism, they generate hot electron-hole pairs in AuHA.[5–8,53,61] The decay time and length of Landau damped plasmons are ~1 to 100 fs and ~1 nm, respectively.[3,61,62] With the electromagnetic field intensity due to plasmons being high at the hole edges [Figs. 2(c) and 2(d)], an initial population of hot electrons confined very close to the edge of the holes is generated from the plasmon decay within the pulse duration. This gives rise to a nonuniform distribution of hot carriers between the holes. The hot carriers diffuse from their high density regions to form spatially uniform distribution of hot electrons. The characteristic hot carrier diffusion time is given by $\tau_d = C_e l^2/2\kappa_e$, where $C_e = 1.98 \times 10^4$ Jm^{-3} K^{-1} and $\kappa_e = 310$ Wm^{-1} K^{-1} are electronic specific heat and thermal conductivity of gold, respectively.[53] Taking $l = 260$ nm as the half of the distance between the edges of two adjacent holes, we get an estimate $\tau_d \sim 2.2$ ps. As the diffusion time τ_d and carrier cooling time τ_p are comparable, an increase of 1 ps in τ_p can be possibly attributed to the diffusion of hot carriers. In addition, as the plasmon-induced hot carriers in graphene are generated through the hole edges (or plasmonic hotspots) in contact with graphene, hot carriers generated are initially nonuniformly distributed in graphene. The hot carriers in graphene also take finite time to diffuse and form a uniform distribution between the plasmonic hotspots. The diffusion coefficient of hot carriers in CVD graphene is $D_e = 5.5 \times 10^3$ cm^2 s^{-1}.[63] The characteristic diffusion time of hot carriers estimated by $\tau_d = l^2/2D_e$ gives $\tau_d = 57$ fs for = 250 nm (half of the average distance between hole edges or plasmonic hotspots). The fast diffusion ensures uniform distribution hot carriers in graphene within the pump pulse duration. Therefore, the presence of graphene has no effect on τ_p in G-AuHA. However, a slightly reduced value of τ_p is observed in G-Au in comparison to the Au film. As graphene is in more contact with the Au film, it modifies the decay rate to the effective decay rate ($1/\tau_{eff} = 1/\tau_p + 1/\tau_G$) and therefore results in a slightly faster decay.[64]

A comparison of ultrafast carrier dynamics also helps us in identifying the direct or indirect nature of the plasmon-induced hot carrier generation in graphene. If the transfer pathway of hot carriers in graphene is indirect [due to the near-field interaction of graphene with gold[22] or plasmon-induced hot electron transfer (PHET)[10]], the carrier dynamics in graphene must be affected by the diffusion dynamics of hot carriers in AuHA and should show a slower decay dynamics. However, as the time constant τ_G observed by us in G-AuHA agrees with that reported for CVD graphene on the quartz substrate,[54] we conclude that the transfer pathway of plasmon-induced hot carriers in graphene in the G-AuHA system is direct. The back transfer of hot carriers to Au is prevented by spatially separating them from the plasmonic hot spots (protruding edges of the holes).

IV. CONCLUSION

In conclusion, we have studied the photoexcited carrier dynamics of the hybrid plasmonic structure of the graphene-covered gold hole array to study the graphene-plasmon interaction. Graphene on the 3D hole array of gold shows strong coupling to the plasmonic modes. We have shown that plasmon-induced hot carriers can be

Published under license by AIP Publishing

efficiently generated in graphene. The frequency tuning of EOT resonances in the Au hole array (by changing the hole spacing) is a very attractive possibility to inject hot carriers in graphene in spectral regions other than the plasmon resonances in noble metals in the visible region. Our results have interesting technological implications in hot carrier devices with tunable photon energy. The hot electrons once separated from the plasmonic hot spots can be utilized in surface catalytic reactions and optoelectronic devices. Similar to the reported photocatalysis using visible light overlapping with the surface plasmon resonance of the Au nanoparticles covered with graphene oxide,[20] we propose that a photocatalysis should be possible by graphene covered AuHA using photons of energy close to other plasmonic resonances of the AuHA (0.8–1.6 eV).

ACKNOWLEDGMENTS

G.P. and S.N.G. would like to thank the Council of Scientific and Industrial Research (CSIR) for Senior Research Fellowship (SRF). A.K.S. and R.K.S. would like to thank the Nanomission Council of the Department of Science and Technology, Government of India, for financial support.

REFERENCES

[1] C. Genet and T. W. Ebbesen, "Light in tiny holes," Nature **445**, 39 (2007).
[2] W. L. Barnes, A. Dereux, and T. W. Ebbesen, "Surface plasmon subwavelength optics," Nature **424**, 824 (2003).
[3] M. L. Brongersma, N. J. Halas, and P. Nordlander, "Plasmon-induced hot carrier science and technology," Nat. Nanotechnol. **10**, 25 (2015).
[4] C. Clavero, "Plasmon-induced hot-electron generation at nanoparticle/metal-oxide interfaces for photovoltaic and photocatalytic devices," Nat. Photonics **8**, 95 (2014).
[5] M. Moskovits, "The case for plasmon-derived hot carrier devices," Nat. Nanotechnol. **10**, 6 (2015).
[6] S. Link and M. A. El-Sayed, "Size and temperature dependence of the plasmon absorption of colloidal gold nanoparticles," J. Phys. Chem. B **103**, 4212 (1999).
[7] C. Sönnichsen, T. Franzl, T. Wilk, G. von Plessen, J. Feldmann, O. V. Wilson, and P. Mulvaney, "Drastic reduction of plasmon damping in gold nanorods," Phys. Rev. Lett. **88**, 077402 (2002).
[8] S. Link and M. A. El-Sayed, "Shape and size dependence of radiative, non-radiative and photothermal properties of gold nanocrystals," Int. Rev. Phys. Chem. **19**, 409 (2000).
[9] R. Tsu, "Landau damping and dispersion of phonon, plasmon, and photon waves in polar semiconductors," Phys. Rev. **164**, 380 (1967).
[10] K. Wu, J. Chen, J. R. McBride, and T. Lian, "Efficient hot-electron transfer by a plasmon-induced interfacial charge-transfer transition," Science **349**, 632 (2015).
[11] R. Sundararaman, P. Narang, A. S. Jermyn, W. A. Goddard III, and H. A. Atwater, "Theoretical predictions for hot-carrier generation from surface plasmon decay," Nat. Commun. **5**, 5788 (2014).
[12] C. Ropers, D. J. Park, G. Stibenz, G. Steinmeyer, J. Kim, D. S. Kim, and C. Lienau, "Femtosecond light transmission and subradiant damping in plasmonic crystals," Phys. Rev. Lett. **94**, 113901 (2005).
[13] S. V. Boriskina, H. Ghasemi, and G. Chen, "Plasmonic materials for energy: From physics to applications," Mater. Today **16**, 375 (2013).
[14] T. V. Shahbazyan, "Landau damping of surface plasmons in metal nanostructures," Phys. Rev. B **94**, 235431 (2016).
[15] A. O. Govorov, H. Zhang, and Y. K. Gun'ko, "Theory of photoinjection of hot plasmonic carriers from metal nanostructures into semiconductors and surface molecules," J. Phys. Chem. C **117**, 16616 (2013).
[16] G. V. Hartland, "Optical studies of dynamics in noble metal nanostructures," Chem. Rev. **111**, 3858 (2011).
[17] K. S. Novoselov, A. K. Geim, S. V. Morozov, D. Jiang, Y. Zhang, S. V. Dubonos, I. V. Grigorieva, and A. A. Firsov, "Electric field effect in atomically thin carbon films," Science **306**, 666 (2004).
[18] Y. Zhang, Y. W. Tan, H. L. Stormer, and P. Kim, "Experimental observation of the quantum Hall effect and Berry's phase in graphene," Nature **438**, 201 (2005).
[19] A. N. Grigorenko, M. Polini, and K. S. Novoselov, "Graphene plasmonics," Nat. Photonics **6**, 749 (2012).
[20] D. Kumar, A. Lee, T. Lee, M. Lim, and D.-K. Lim, "Ultrafast and efficient transport of hot plasmonic electrons by graphene for Pt free, highly efficient visible-light responsive photocatalyst," Nano Lett. **16**, 1760 (2016).
[21] A. Hoggard, L.-Y. Wang, L. Ma, Y. Fang, G. You, J. Olson, Z. Liu, W. S. Chang, P. M. Ajayan, and S. Link, "Using the plasmon linewidth to calculate the time and efficiency of electron transfer between gold nanorods and graphene," ACS Nano **7**, 11209 (2013).
[22] A. M. Gilbertson, Y. Francescato, T. Roschuk, V. Shautsova, Y. Chen, T. P. Sidiropoulos, M. Hong, V. Giannini, S. A. Maier, L. F. Cohen *et al.*, "Plasmon-induced optical anisotropy in hybrid graphene-metal nanoparticle systems," Nano Lett. **15**, 3458 (2015).
[23] H. Shan, Y. Yu, X. Wang, Y. Luo, S. Zu, B. Du, T. Han, B. Li, Y. Li, J. Wu *et al.*, "Direct observation of ultrafast plasmonic hot electron transfer in the strong coupling regime," Light: Sci. Appl. **8**, 9 (2019).
[24] H. Shan, Y. Yu, R. Zhang, R. Cheng, D. Zhang, Y. Luo, X. Wang, B. Li, S. Zu, F. Lin *et al.*, "Electron transfer and cascade relaxation dynamics of graphene quantum dots/MoS_2 monolayer mixed-dimensional van der Waals heterostructures," Mater. Today **24**, 10–16 (2019).
[25] T. W. Ebbesen, H. J. Lezec, H. F. Ghaemi, T. Thio, and P. A. Wolff, "Extraordinary optical transmission through sub-wavelength hole arrays," Nature **391**, 667 (1998).
[26] D. Psaltis, S. R. Quake, and C. Yang, "Developing optofluidic technology through the fusion of microfluidics and optics," Nature **442**, 381 (2006).
[27] A. E. Cetin, A. F. Coskun, B. C. Galarreta, M. Huang, D. Herman, A. Ozcan, and H. Altug, "Handheld high-throughput plasmonic biosensor using computational on-chip imaging," Light: Sci. Appl. **3**, e122 (2014).
[28] C. Escobedo, "On-chip nanohole array based sensing: A review," Lab Chip **13**, 2445 (2013).
[29] X. Zhu, L. Shi, M. S. Schmidt, A. Boisen, O. Hansen, J. Zi, S. Xiao, and N. A. Mortensen, "Enhanced light-matter interactions in graphene-covered gold nanovoid arrays," Nano Lett. **13**, 4690 (2013).
[30] N. Reckinger, A. Vlad, S. Melinte, J.-F. Colomer, and M. Sarrazin, "Graphene-coated holey metal films: Tunable molecular sensing by surface plasmon resonance," Appl. Phys. Lett. **102**, 211108 (2013).
[31] Q. Hao, B. Wang, J. A. Bossard, B. Kiraly, Y. Zeng, I.-K. Chiang, L. Jensen, D. H. Werner, and T. J. Huang, "Surface-enhanced Raman scattering study on graphene-coated metallic nanostructure substrates," J. Phys. Chem. C **116**, 7249 (2012).
[32] J. Zhang, M. Irannejad, M. Yavuz, and B. Cui, "Gold nanohole array with sub-1 nm roughness by annealing for sensitivity enhancement of extraordinary optical transmission biosensor," Nanoscale Res. Lett. **10**, 238 (2015).
[33] C. Genslein, P. Hausler, E.-M. Kirchner, R. Bierl, A. J. Baeumner, and T. Hirsch, "Graphene-enhanced plasmonic nanohole arrays for environmental sensing in aqueous samples," Beilstein J. Nanotechnol. **7**, 1564 (2016).
[34] A. Mahigir, T.-W. Chang, A. Behnam, G. L. Liu, M. R. Gartia, and G. Veronis, "Plasmonic nanohole array for enhancing the SERS signal of a single layer of graphene in water," Sci. Rep. **7**, 14044 (2017).
[35] Y. Zhao, D. Yang, X. Li, Y. Liu, X. Hu, D. Zhou, and Y. Lu, "Toward highly sensitive surface-enhanced Raman scattering: The design of a 3D hybrid system with monolayer graphene sandwiched between silver nanohole arrays and gold nanoparticles," Nanoscale **9**, 1087 (2017).
[36] H. Fredriksson, Y. Alaverdyan, A. Dmitriev, C. Langhammer, D. S. Sutherland, M. Zäch, and B. Kasemo, "Hole-mask colloidal lithography," Adv. Mater. **19**, 4297 (2007).
[37] S. Kar, D. R. Mohapatra, E. Freysz, and A. K. Sood, "Tuning photoinduced terahertz conductivity in monolayer graphene: Optical-pump terahertz-probe spectroscopy," Phys. Rev. B **90**, 165420 (2014).

Published under license by AIP Publishing

[38]C. N. R. Rao, A. K. Sood, K. S. Subrahmanyam, and A. Govindaraj, "Graphene: The new two-dimensional nanomaterial," Angew. Chem., Int. Ed. **48**, 7752 (2009).
[39]A. Das, S. Pisana, B. Chakraborty, S. Piscanec, S. K. Saha, U. V. Waghmare, K. S. Novoselov, H. R. Krishnamurthy, A. K. Geim, A. C. Ferrari *et al.*, "Monitoring dopants by Raman scattering in an electrochemically top-gated graphene transistor," Nat. Nanotechnol. **3**, 210 (2008).
[40]R. Yan, Q. Zhang, W. Li, I. Calizo, T. Shen, C. A. Richter, A. R. Hight-Walker, X. Liang, A. Seabaugh, D. Jena *et al.*, "Determination of graphene work function and graphene-insulator-semiconductor band alignment by internal photoemission spectroscopy," Appl. Phys. Lett. **101**, 022105 (2012).
[41]P. A. Anderson, "Work function of gold," Phys. Rev. **115**, 553 (1959).
[42]F. Cerdeira, T. A. Fjeldly, and M. Cardona, "Effect of free carriers on zone-center vibrational modes in heavily doped p-type Si. II. Optical modes," Phys. Rev. B **8**, 4734 (1973).
[43]S. D. M. Brown, A. Jorio, P. Corio, M. S. Dresselhaus, G. Dresselhaus, R. Saito, and K. Kneipp, "Origin of the Breit-Wigner-Fano lineshape of the tangential G-band feature of metallic carbon nanotubes," Phys. Rev. B **63**, 155414 (2001).
[44]D. Yoon, D. Jeong, H.-J. Lee, R. Saito, Y.-W. Son, H. C. Lee, and H. Cheong, "Fano resonance in Raman scattering of graphene," Carbon **61**, 373 (2013).
[45]B. Ai, Y. Yu, H. Möhwald, and G. Zhang, "Novel 3D Au nanohole arrays with outstanding optical properties," Nanotechnology **24**, 035303 (2012).
[46]S. B. Quint and C. Pacholski, "Getting real: Influence of structural disorder on the performance of plasmonic hole array sensors fabricated by a bottom-up approach," J. Mater. Chem. C **2**, 7632 (2014).
[47]A. Devizis, V. Vaicikauskas, and V. Gulbinas, "Ultrafast pump-probe surface plasmon resonance spectroscopy of thin gold films," Appl. Opt. **45**, 2535 (2006).
[48]S. Link, C. Burda, Z. L. Wang, and M. A. El-Sayed, "Electron dynamics in gold and gold-silver alloy nanoparticles: The influence of a nonequilibrium electron distribution and the size dependence of the electron–phonon relaxation," J. Chem. Phys. **111**, 1255 (1999).
[49]M. Aeschlimann, S. Pawlik, and M. Bauer, "Femtosecond time-resolved measurement of electron relaxation at metal surfaces," Ber. Bunsen-Ges. Phys. Chem. **99**, 1504 (1995).
[50]S. Pawlik, M. Bauer, and M. Aeschlimann, "Lifetime difference of photoexcited electrons between intraband and interband transitions," Surf. Sci. **377**, 206 (1997).
[51]C. K. Sun, F. Vallée, L. H. Acioli, E. P. Ippen, and J. G. Fujimoto, "Femtosecond-tunable measurement of electron thermalization in gold," Phys. Rev. B **50**, 15337 (1994).
[52]G. L. Eesley, "Observation of nonequilibrium electron heating in copper," Phys. Rev. Lett. **51**, 2140 (1983).
[53]R. H. M. Groeneveld, R. Sprik, and A. Lagendijk, "Femtosecond spectroscopy of electron-electron and electron-phonon energy relaxation in Ag and Au," Phys. Rev. B **51**, 11433 (1995).
[54]J. Shang, T. Yu, J. Lin, and G. G. Gurzadyan, "Ultrafast electron-optical phonon scattering and quasiparticle lifetime in CVD-grown graphene," ACS Nano **5**, 3278 (2011).
[55]K.-C. Huang, J. McCall, P. Wang, C.-S. Liao, G. Eakins, J.-X. Cheng, and C. Yang, "High-speed spectroscopic transient absorption imaging of defects in graphene," Nano Lett. **18**, 1489 (2018).
[56]T. Ando, "Zero-mode anomalies of massless Dirac electron in graphene," J. Appl. Phys. **109**, 102401 (2011).
[57]L. Guo and X. Xu, "Ultrafast spectroscopy of electron-phonon coupling in gold," J. Heat Transfer **136**, 122401 (2014).
[58]X. D. Li, T. P. Chen, Y. Liu, and K. C. Leong, "Influence of localized surface plasmon resonance and free electrons on the optical properties of ultrathin Au films: A study of the aggregation effect," Opt. Express **22**, 5124 (2014).
[59]R. Lässer and N. V. Smith, "Interband optical transitions in gold in the photon energy range 2-25 eV," Solid State Commun. **37**, 507 (1981).
[60]M. Zhou, C. Zeng, Y. Chen, S. Zhao, M. Y. Sfeir, M. Zhu, and R. Jin, "Evolution from the plasmon to exciton state in ligand-protected atomically precise gold nanoparticles," Nat. Commun. **7**, 13240 (2016).
[61]M. Bernardi, J. Mustafa, J. B. Neaton, and S. G. Louie, "Theory and computation of hot carriers generated by surface plasmon polaritons in noble metals," Nat. Commun. **6**, 7044 (2015).
[62]C. Jia, X. Li, N. Xin, Y. Gong, J. Guan, L. Meng, S. Meng, and X. Guo, "Interface-engineered plasmonics in metal/semiconductor heterostructures," Adv. Energy Mater. **6**, 1600431 (2016).
[63]B. A. Ruzicka, S. Wang, J. Liu, K.-P. Loh, J. Z. Wu, and H. Zhao, "Spatially resolved pump-probe study of single-layer graphene produced by chemical vapor deposition," Opt. Mater. Express **2**, 708 (2012).
[64]D. Brida, A. Tomadin, C. Manzoni, Y. J. Kim, A. Lombardo, S. Milana, R. R. Nair, K. S. Novoselov, A. C. Ferrari, G. Cerullo *et al.*, "Ultrafast collinear scattering and carrier multiplication in graphene," Nat. Commun. **4**, 1987 (2013).

Published under license by AIP Publishing